ADVANCED MATERIALS INTERFACES
www.advmatinterfaces.de

Effect of Electrolyte Additives on the $LiNi_{0.5}Mn_{0.3}Co_{0.2}O_2$ Surface Film Formation with Lithium and Graphite Negative Electrodes

Maral Hekmatfar, Ivana Hasa, Ramtin Eghbal, Diogo V. Carvalho, Arianna Moretti, and Stefano Passerini**

The effect of various electrolyte additives (fluoroethylene carbonate (FEC), vinylene carbonate (VC), and propane sultone (PS)) on the performance of $LiNi_{0.5}Mn_{0.3}Co_{0.2}O_2$ (NMC532) electrodes in combination with lithium (half-cell) and graphite (full-cell) negative electrodes, is herein reported. The cathode/electrolyte interface (CEI) layer formed on the NMC532 electrode cycled up to 4.5 V versus Li^+/Li is investigated by X-ray photoelectron spectroscopy and scanning electron microscopy. This allows correlating the electrochemical performance of the electrodes to the CEI chemical composition, thickness, and morphology. All the investigated electrolyte additives exhibit beneficial effects in half- and full-cell systems, confirming the effective passivation layer formation protecting the electrolyte from further decomposition at high voltages. It is found that the thickness of the CEI layer forming on the NMC532 electrodes in half- and full-cell configuration is different. VC and PS are found to be the best additives to enhance the performance mainly due to their positive contribution to the CEI formation. The solid/electrolyte interphase (SEI) formed on the graphite electrode is also investigated and compared to the CEI layer formed on the cathode. The detection of typical SEI reduction products on the positive electrode surface confirms the occurrence of cross-talking between the two electrodes.

1. Introduction

Lithium-ion batteries (LIBs) have experienced a widely increasing deployment in the automotive sector due to their superior power and energy performance compared to other battery chemistries, enabling reduced weight and dimensions at competitive prices.[1–3]

Since their introduction in the market,[4,5] the attention of both Academia and Industry has been dedicated to the improvement of LIBs' performance.[6] The continuing optimization of energy density, cycle life, and safety has enabled the widespread use of LIBs in a variety of application fields, such as portable and wearable electronics, stationary storage, and electrified transportation. To satisfy the continuously increasing demand on high gravimetric and volumetric energy density, high voltage and high capacity materials have been intensively studied in combination with other optimized cell components.[7–9] Among the positive electrodes, layered lithium nickel manganese cobalt oxides ($LiNi_xMn_yCo_zO_2$, NMC with $x + y + z = 1$) have been extensively studied due to the lower cost and higher specific capacity compared to $LiCoO_2$ and the good structural stability characterized by a small volume change (less than 2%) during Li insertion/extraction.[10–12]

Despite the theoretical capacity of NMC is as high as 275 mAh g^{-1}, not all lithium can be extracted from the structure without encountering structural instability and degradation.[13]

In order to achieve higher capacities and increase the discharge voltage, i.e., improving the energy performance while simultaneously reducing the environmental impact and cost, a variety of NMC composition has been developed. Indeed, by increasing the Ni content[14–16] and reducing the amount of the more expensive and toxic Co,[17,18] a series of $LiNi_xMn_yCo_zO_2$ ($x + y + z = 1$) materials has been synthesized, which are named after the ratio of the transition metals (x:y:z = 1:1:1, NMC; 4:4:2, NMC442; 5:3:2, NMC532; 6:2:2, NMC622; and 8:1:1, NMC811).[14–19]

All transition metals in the NMC materials contribute with pros and cons to the overall properties. Indeed, high Ni content increases the material's capacity, but also leads to high preparation complexity, structural instability (due to the Li^+/Ni^{2+} cation mixing), and exacerbated cathode/electrolyte interface (CEI) instability.[20] On the other side, increasing Mn content leads

M. Hekmatfar, Dr. I. Hasa, R. Eghbal, Dr. D. V. Carvalho, Dr. A. Moretti, Prof. S. Passerini
Helmholtz Institute Ulm (HIU)
Helmholtzstrasse 11, 89081 Ulm, Germany
E-mail: ivana.hasa@kit.edu; stefano.passerini@kit.edu
M. Hekmatfar, Dr. I. Hasa, R. Eghbal, Dr. D. V. Carvalho, Dr. A. Moretti, Prof. S. Passerini
Karlsruhe Institute of Technology (KIT)
P.O. Box 3640, 76021 Karlsruhe, Germany
The ORCID identification number(s) for the author(s) of this article can be found under https://doi.org/10.1002/admi.201901500.

© 2019 Karlsruhe Institute of Technology. Published by WILEY-VCH Verlag GmbH & Co. KGaA, Weinheim. This is an open access article under the terms of the Creative Commons Attribution-NonCommercial-NoDerivs License, which permits use and distribution in any medium, provided the original work is properly cited, the use is non-commercial and no modifications or adaptations are made.

DOI: 10.1002/admi.201901500

to improved structural stability, but lower capacity.[21–25] Finally, Co incorporation strongly improves the rate performance[20] besides increasing the structural stability by mitigating the Li^+/Ni^{2+} cation mixing,[26] but it increases cost and harmfulness.

In general, increasing the Ni content in NMC results in higher capacity, more Li can be reversibly extracted/inserted from/in the layered NMC structure, within the same voltage window. Higher performance can be obtained by increasing the upper cut-off voltage, however, this approach aggravates the oxidative processes of the electrolyte. These latter lead to continuous electrolyte decomposition accompanied by thicker surface films formation and with consequent charge-transfer impedance increase, gas evolution and transition metal dissolution are ultimately affecting the cycling stability and even causing cell failure.[20,27–29]

For such reasons, the working voltage of NMC-based positive electrodes is nowadays limited to ≈4.3 V.[11] A commonly employed strategy to improve the stability of the CEI consists in the realization of a protective coating layer on the active material particles.[30,31] However, this requires modification of the synthesis method or additional post-processing of the NMC particles. Another effective approach is the introduction of additives in the electrolyte formulation, which would in situ form a CEI thus reducing or even supressing the electrolyte reactions at the electrode interface at high voltages. Indeed, additives are the key to enable the use of graphite (Gr) anodes by improving the chemical and mechanical stability through the formation of the solid/electrolyte interphase (SEI) during the first few cycles of LIBs.[32] Also, flame-retardant and redox shuttle additives increase the safety of LIBs.[8,33,34]

Vinylene carbonate (VC) is a well-known electrolyte component employed in LIBs as SEI forming additive.[35–40] VC is reduced during the first cathodic scan at relatively high voltage forming polymeric compounds, which generate a stable, poorly electronically conductive passivation film on the graphite particles hindering further solvent decomposition.[35] The SEI composition is also relatively depleted from lithium alkyl carbonates and LiF which are generated from the reduction of cyclic carbonates and salt decomposition, respectively, at more cathodic voltages than VC.[41] Also, because of the larger fraction of polymeric compounds, the VC-based SEI is rather flexible, offering a better accommodation of graphite's volume changes and preventing a continuous irreversible consumption of Li ions.[35] Aurbach et al. reported that VC-containing electrolytes also increase the cell cyclability and improve the thermal properties of SEI.[35] In spite of all the beneficial effects, excessive amounts of VC in the electrolyte lead to increased charge transfer resistance at the negative electrode, thus VC should be carefully dosed (usually limited to 1–2 wt%).[42] Recently, it has been demonstrated that VC has also a positive impact on the CEI formation. Burns et al. reported decreased rates of electrolyte oxidation at the $LiCoO_2$ (LCO) surface in the presence of VC.[43] Moreover, polymeric VC, namely, poly(VC), was also detected at the surface of NMC[44,45] and LCO electrodes.[46] The presence of poly(VC) was explained by the occurrence of an oxidative decomposition occurring via a radical polymerization of VC, similarly to the process occurring at the negative electrode.[46] Interestingly, while poly(VC) species were detected on the surface of LCO (at 4.2 V), they were not observed on that of $LiFePO_4$ electrodes charged up to 4.5 V, suggesting a specific catalytic activity of the transition metals toward VC oxidation through nucleophilic attack.[47]

Sulphur-based additives, such as sultones, are also known to be effective SEI forming agents improving the thermal and cycling stability of LIB.[48–50] Studies conducted on 1 wt% addition of 1,3-propane sultone (PS) in LR-NMC//Li and LR-NMC//Gr cells suggested that a protective layer formation on active material particles due to PS decomposition preserves the material integrity and mitigates Mn^{2+} dissolution into the electrolyte.[51]

In addition, reduced gas evolution upon formation cycling was detected in graphite//Li cells employing 2 wt% PS added electrolyte. Moreover, the improved ionic conductivity observed for the SEI formed in NMC//Gr cells was attributed to the presence of lithium alkylsufonate species originated from PS decomposition.[34]

Fluoroethylene carbonate (FEC) has been also intensively studied especially in combination with graphite and silicon electrodes due to its beneficial effect on the formation of an optimal SEI layer resulting in cell performance improvement.[52–55] Wang et al. showed that FEC enhances the Coulombic efficiency (CE) and long-term cycling of LCO//Gr pouch cells, also reducing the charge end point capacity slippage and self-discharge during storage, when compared to cells with additive-free electrolyte.[56] Further studies conducted by Shin et al. reported on the effect of FEC at the interface of both the positive and negative electrodes of $LiMn_2O_4$ (LMO)//Gr cells at room temperature and 55 °C. In particular, at room temperature FEC exerted a positive effect on the graphite SEI reflected in improved capacity retention, while for LMO almost no variation was observed. On the other side at 55 °C while the SEI on graphite was still stable, on the LMO side, poor cycle retention and increased interfacial resistance occurred, most likely due to the formation of a thicker CEI and the increased Mn dissolution accelerated by hydrogen fluoride (HF).[55] Xu et al. recently revealed that while FEC can form a robust SEI on the electrode, it also deteriorates the shelf life of electrolytes containing $LiPF_6$. By using liquid- and solid-state NMR, it has been demonstrated that traces of water residues induce hydrolysis of $LiPF_6$, releasing HF and PF_5 which further trigger ring-opening of FEC and its subsequent polymerization. The reactions are significantly accelerated at elevated temperatures leading to the formation of a 3D fluorinated solid polymer network.[57] Qian et al. showed that FEC improves the electrochemical performance of NMC in half-cell cycled up to 4.2 V (vs Li/Li^+) when compared to VC and ethylene sulfite additives. X-ray photoelectron spectroscopy (XPS) measurements showed that the FEC-containing electrolyte induces the thinnest CEI layer, mostly consisting of LiF.[58] Li et al. recently showed that the combination of FEC with ethylene sulfate (DTD) improves the lifetime of single crystal NMC(532)//artificial graphite cells at 4.4 V by improving the electrolyte stability at high voltages and by exhibiting a relatively low difference between the average charge and discharge voltage (≈0.007(1) V) after 850 cycles.[59]

All the above-mentioned studies suggest that a rational electrolyte design is crucial for the development of high performance, long lasting LIBs. However, a successful electrolyte design requires the detailed investigation of both SEI and CEI properties upon different cycling conditions, in particular the upper cut-off potential.

In this work, the effect of three additives, VC, PS, and FEC, is evaluated in relation to the CEI and SEI layer composition and to the cell performance at high voltage (4.5 V). The study

© 2019 Karlsruhe Institute of Technology. Published by WILEY-VCH Verlag GmbH & Co. KGaA, Weinheim

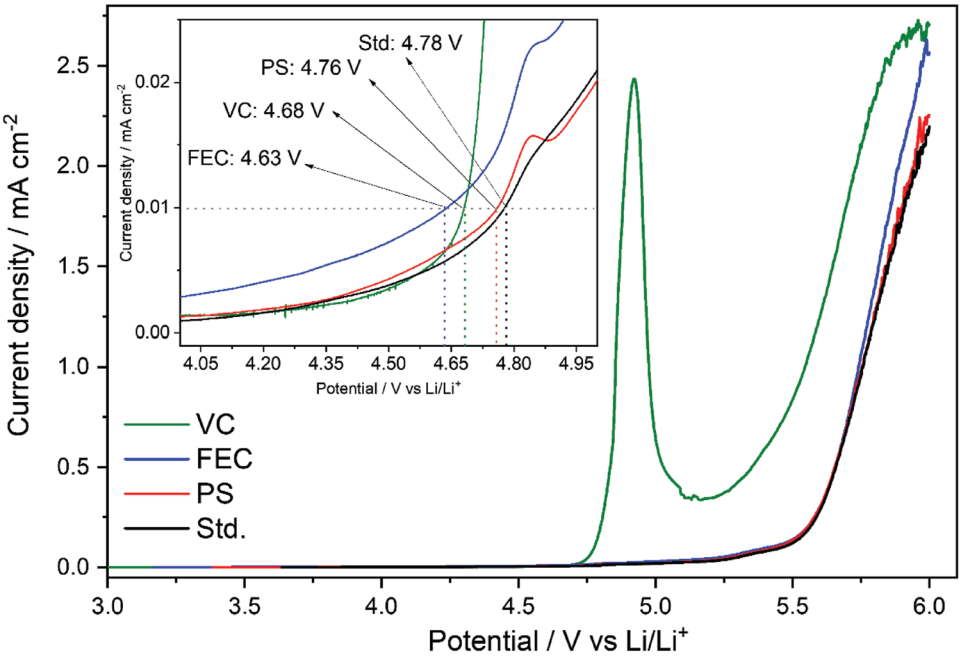

Figure 1. Anodic stability of the investigated electrolytes determined by using carbon black-based electrode as working electrode. Test run at 0.1 mV s^{-1} at room temperature. Inset: enlarged region highlighting the oxidative current limit of 10 µA cm^{-2} as the threshold for the anodic stability.

has been carried out combining electrochemical tests and XPS providing insights into the mechanisms of the CEI layer formation on NMC532 in combination with lithium and graphite negative electrodes.

2. Results and Discussion

2.1. Electrolyte Characterization

The anodic stability of the electrolytes was investigated using carbon black-based electrodes. These have been chosen to simulate more realistic cell conditions with respect to the commonly employed inert electrodes, such as platinum,[60] which generally gives higher anodic stability values. **Figure 1** shows the linear sweep voltammograms of the four electrolytes from open circuit potential (OCP) to 6 V obtained at a scan rate of 0.1 mV s^{-1}.

At a first glance, VC exhibits a sharp oxidation peak at ≈4.7 V versus Li^+/Li, while the other three electrolytes show smoother increase of the anodic current only after 5 V. However, the inset of Figure 1, reporting the enlarged potential versus current profiles, shows that all electrolytes exhibit anodic decomposition processes at rather lower potentials. Setting the oxidative current limit to 10 µA cm^{-2}, the anodic stability of the electrolytes follows the order: Std > PS > VC > FEC.

In more details, FEC shows the highest oxidative decomposition current reaching the 10 µA cm^{-2} threshold at 4.63 V versus Li^+/Li. Afterward, the current increases rather slowly depicting a shoulder at about 4.82 V versus Li^+/Li. VC reaches the oxidative decomposition current threshold at 4.68 V versus Li^+/Li, but the current increases dramatically at 4.7 V versus Li^+/Li. Std reaches the oxidative current limit at 4.76 V versus Li^+/Li and further exhibits a small current increase at about 4.82 V versus Li^+/Li similarly to FEC. Finally, PS reaches the threshold at 4.76 V versus Li^+/Li. In summary, the anodic stability of all four electrolytes largely exceeds 4.6 V versus Li^+/Li, but the addition of VC or FEC causes a slight decrease with respect to Std.

2.2. Electrochemical Performance of NMC532//Li Cells

The electrochemical behavior of NMC532 electrodes in combination with lithium (half-cell) has been investigated by galvanostatic cycling tests performed within the 3.0–4.5 V voltage range. All cells were subjected to the formation protocol consisting of a first cycle at C/20 rate followed by two other cycles at C/10 rate.

Figure 2 reports the 1st charge–discharge voltage profiles (C/20) for the cells containing the four different electrolytes. The cells exhibit discharge capacities of about 195, 195.6, 196.3, and 197.9 mAh g^{-1}, respectively, for FEC, VC, PS, and Std. The respective CEs reached about 90%, 89.3%, 91.3%, and 91.6% as a result of the electrolyte decomposition and other irreversible reactions occurring at the electrode/electrolyte interface. The inset in Figure 2 shows the sharp decrease of the irreversible capacity in the second and third cycles confirming the decreased decomposition processes. After the formation cycles, the cells were galvanostatically cycled at 1 C rate.

Overall, PS and VC containing cells exhibit stable cycling performance over about 30 cycles while FEC and Std lead to slightly inferior performance, as shown in **Figure 3** reporting the cycling behavior in terms of delivered capacity and CE. After 30 cycles at 1 C, the CE increases to 99.86% (VC), 99.70% (PS), 99.87% (FEC), and 98.39% (Std), indicating the beneficial effects of the additives upon cycling when compared to the standard electrolyte.

© 2019 Karlsruhe Institute of Technology. Published by WILEY-VCH Verlag GmbH & Co. KGaA, Weinheim

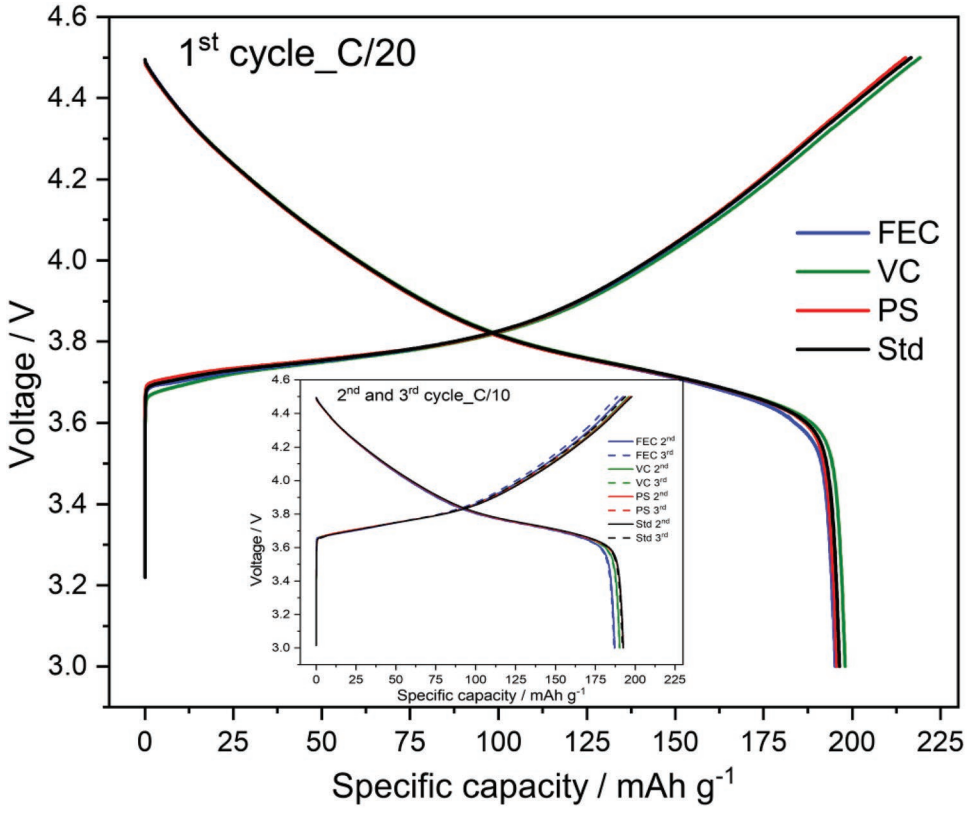

Figure 2. Voltage profile of NMC532//Li cells employing Std, PS, VC, and FEC during the formation protocol. 1st cycle run at C/20 and two following cycles (in inset) at C/10. Test run at room temperature. Voltage range: 3.0–4.5 V.

The use of VC and PS additive clearly improves the cycling stability and CE. Indeed, Std and FEC containing cells exhibit a capacity retention of 96.3% and 95.7%, while VC and PS improve the values up to 97.6% and 99%, respectively.

Generally, the delivered capacity decrease can be associated with the overall cell impedance increase or lithium inventory loss.[61–63] This latter, however, does not apply for half-cells since the Li metal electrode guarantees a large inventory excess.

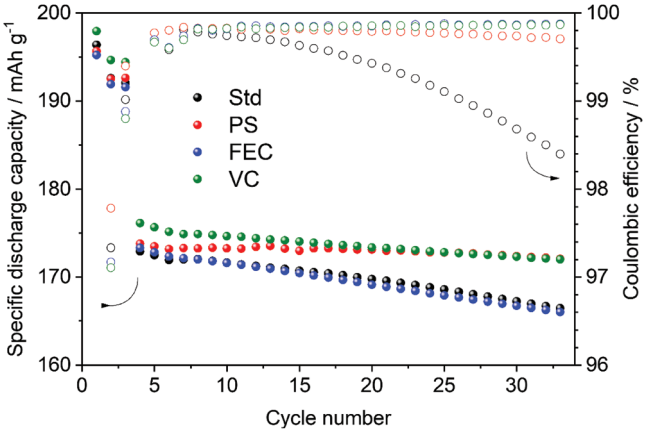

Figure 3. Cycling performance at 1 C (including formation cycles at C/20 and C/10) of NMC532//Li cells employing Std, PS, VC, and FEC. Test run at room temperature. Voltage range: 3.0–4.5 V.

Figure 4 shows selected voltage profiles, namely, the 4th, 14th, 24th, and 33rd cycle for the cells cycled with the four different electrolytes. The voltage profile of the cell employing Std clearly exhibits an increased cell polarization upon cycling, as evidenced by the increased de-lithiation and decreased lithiation voltages and the increased Ohmic drop. The discharge voltage decay (i.e., upon lithiation) is about 1.3%. A rather comparable behavior is observed for the FEC cell. On the other hand, the PS and VC cells present a very limited Ohmic drop and much smaller voltage decay, resulting in better capacity retention.

Table 1 reports the calculated average lithiation voltage at the 4th cycle, and its decay at the 33rd cycle, also summarizing the capacity retention and CE values for the cycling tests reported in Figure 3.

The improved cycling behavior of the PS- and VC-employing cells is certainly related to the reduced voltage decay upon lithiation when compared to those employing Std or FEC. This can be explained considering that the thickness of the passivation film (CEI) on the NMC532 particles increases upon cycling leading to cell resistance increase (possibly due even to electronic contact loss of the active materials) and thus hindering the de-lithiation/lithiation process.[55]

Overall, the different electrochemical performance offered by the four electrolytes is most likely attributable to the formation of CEIs characterized by different thickness and chemical composition. In order to demonstrate it, post-mortem analysis has been performed and discussed in the following section.

© 2019 Karlsruhe Institute of Technology. Published by WILEY-VCH Verlag GmbH & Co. KGaA, Weinheim

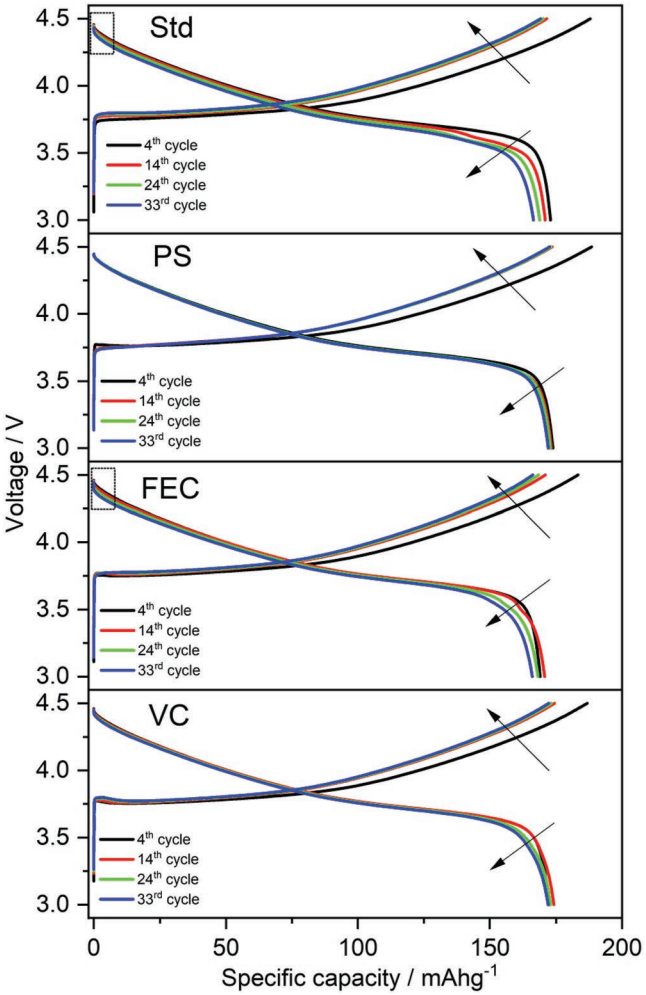

Figure 4. Selected voltage profiles recorded at 1 C rate of NMC532//Li cells employing Std, PS, VC, and FEC. Test run at room temperature. Voltage range: 3.0–4.5 V.

2.3. Post-Mortem XPS Measurements of the Positive Electrodes in NMC532//Li Cells

The improved cycling behavior showed by the cells employing PS and VC can be attributed to the reduced voltage decay upon lithiation and the lower Ohmic drop (i.e., lower cell polarization). These results suggest for a different thickness and chemical composition of the CEI, which was investigated by XPS.

Table 1. Calculated average lithiation voltage, capacity retention, and Coulombic efficiency values for the cycling tests of NMC532//Li cells cycled with Std, PS, VC, and FEC as electrolytes.

	CE at the 33rd cycle/%	Capacity retention (33rd vs 4th cycle)/%	Average lithiation voltage in the 4th cycle/V	Voltage decay after 33 cycles/%
Std	98.39	96.3	3.87	1.3
FEC	99.87	95.7	3.87	0.78
VC	99.86	97.6	3.87	0.26
PS	99.70	99.0	3.86	0.52

Figure 5 shows Mn 2p, O 1s, F 1s, and S 2p core level spectra of the NMC532 electrodes as made (pristine) and after cycling in the four electrolytes. C 1s region is shown in Figure S1 in the Supporting Information.

Mn is electrochemically inactive in NMC532, thus the main peak appearing in the Mn 2p region at about 642 eV, corresponding to Mn^{4+} can be used as an indicator for the thickness of the CEI layer since its intensity is expected to decrease when the CEI layer becomes thicker.

The thickness of the investigated CEI layers can be approximatively calculated considering that the XPS information depth is defined as the depth from which 95.7% of all emitted photoelectrons are able to escape the surface. The maximum obtainable information depth in a photoemission process is defined as $3\lambda_{IMFP}.\cos\theta$,[64] where θ is the angle between the sample surface and collected photoelectrons and λ_{IMFP} is the inelastic mean free path for the electrons. In this case of study, θ is equal to zero, while λ_{IMFP} is calculated to be ≈2.7 and 2 nm for Mn 2p photoelectrons travelling throughout polyethylene-like species and LiF media, respectively.[65,66]

Therefore, according to the calculation, the investigated CEI layers should not exceed 8 nm of thickness since the Mn 2p peak is still slightly observable even for the thicker CEI layers.

As a matter of the fact, the Mn 2p peak of the electrodes cycled in VC and FEC show rather lower intensities than that of the pristine electrode, supporting for a relatively thicker CEI formed in these electrolytes. On the other hand, thinner CEIs are observed for the electrode cycled employing Std and PS.

The X-ray photoelectron spectrum of the pristine electrode in the O 1s region shows two components. The first one, at lower binding energy (529.4 eV), is related to the presence of O^{2-} anions in the oxygen lattice of NMC532 while the second one, at 532.3 eV, is attributed to either oxygen anions with deficient coordination at the NMC532 surface (surface oxygen)[46] and/or residual surface carbonate contamination.[67] Regarding the cycled electrodes, the intensity of the lattice oxygen peak at low binding energy (529.4 eV) is considerably lower for the one exposed to VC and slightly decreased for FEC when compared to PS and Std electrolyte. These results, in good agreement with the observed trend in the Mn 2p region, confirm that VC and FEC generate relatively thicker CEIs on NMC532 surface due to their decomposition and contribution to the layer formation.

For all the electrolytes, a broad feature at about 532.5 eV appears, which overlaps with the peak observed at 532.3 for the pristine electrode.

This broad feature is related to C=O bond containing compounds such as $ROCO_2Li$ (lithium alkylcarbonate) or polycarbonate, resulting from the decomposition of the carbonate solvent.[68,69] In the case of PS, S=O bond containing compounds also contribute to the increased intensity and slight shift toward higher binding energy of this feature.

Another new peak is observed in all the cycled electrodes at ≈534.5 eV. This feature is related to C-O-C bond containing compounds such as polyethyleneoxide-like (PEO) species or, more in general, ROR compounds, once more resulting from the decomposition of the carbonate solvents. In the case of VC, an additional component is observed at about 535 eV indicating the formation of oligo-VC species as a results of the VC oxidative polymerization.[46,70] The formation of poly(VC)

© 2019 Karlsruhe Institute of Technology. Published by WILEY-VCH Verlag GmbH & Co. KGaA, Weinheim

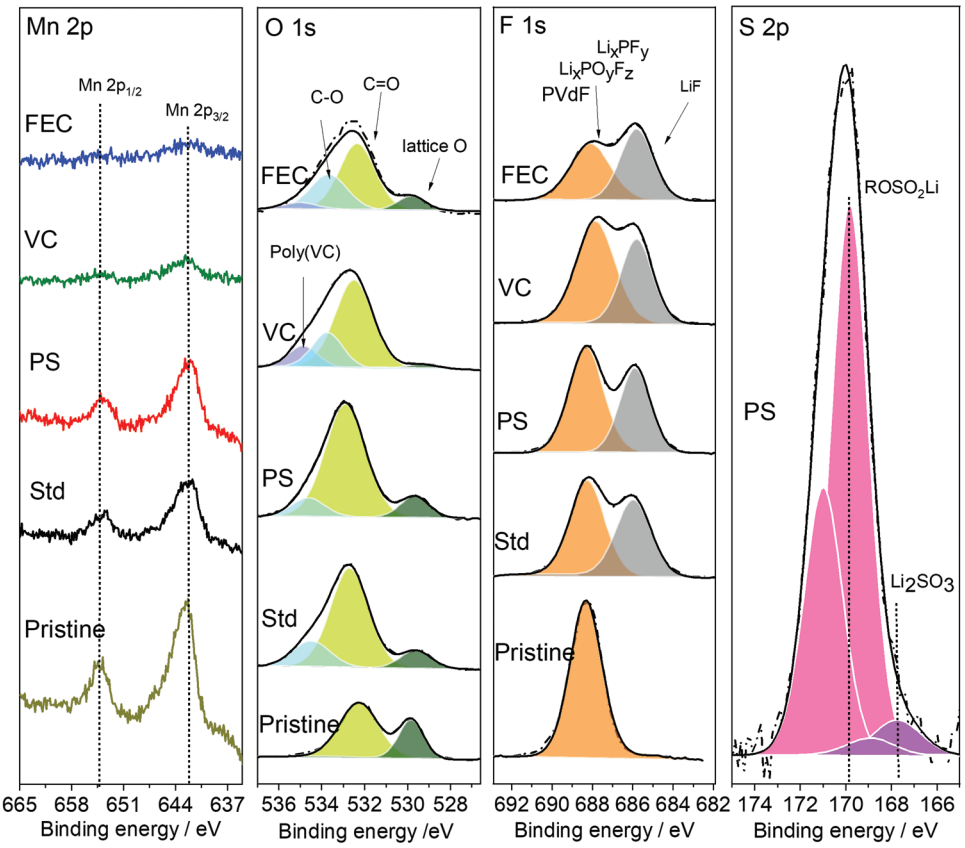

Figure 5. X-ray photoelectron core level spectra of the Mn 2p, O 1s, F 1s, and S 2p region of NMC532 electrodes recovered in the lithiated state after cycling (33rd cycle) from NMC532//Li cells employing Std, PS, VC, and FEC.

species might be responsible for the improved capacity retention observed in VC, linking the improved electrochemical behavior to the more compact and protective surface layer formed on the NMC532 particles.

Similarly, the electrode cycled in FEC shows the feature at about 535 eV associated with the detection of oligo-VC species. The lower peak intensity, however, suggests for a reduced generation of oligo-VC species in the presence of FEC with respect to VC. It has been suggested that FEC can transform into VC by losing HF, which can further polymerize to form polycarbonate species, such as oligo-VC,[8] however, the amount of poly(VC) species formed in the presence of FEC is substantially lower than that with VC suggesting a limited VC polymerization reflected in the inferior electrochemical performances for FEC than VC.

The XPS F 1s spectra of the electrodes are composed of two features. The first one at ≈685.8 eV is assigned to the LiF formed upon degradation of $LiPF_6$.[71,72] The second one at ≈688 eV corresponds to the convoluted contributions of several compounds (PVdF, Li_xPF_y, $Li_xPO_yF_z$), mainly deriving from salt decomposition, but also the binder (see peak for the pristine electrode).[73]

The electrode cycled in FEC exhibits the highest amount of LiF as evidenced by the higher intensity of the peak at low binding energies. This is not the case for the electrodes cycled in the other electrolytes, showing the peak at high binding energies as the most intense. This difference is expected since the decomposition of FEC to form poly(VC) species also generates HF, which, reacting with Li ions, generates additional LiF. This mechanism would also explain the poor electrochemical performance of the FEC-containing cells for two main reasons. First, the FEC decomposition leads to the formation of a thick CEI layer rich in insulating LiF. Second, the HF formation promotes Mn dissolution. It is worth nothing that the adverse effect of FEC on $LiPF_6$-based electrolytes, especially at high temperatures, has been attributed to the dehydrofluorination of FEC which induces more salt decomposition and simultaneous FEC ring-opening polymerization which is catalyzed by HF, deriving from hydrolysis of the $LiPF_6$ salt. The dehydrofluorination reaction is shown in **Scheme 1**.[57]

The XPS S 2p spectrum of the electrode cycled in PS shows two doublets corresponding to $2p_{3/2}$ and $2p_{1/2}$, which are separated by 1.19 eV. The detection of S on the electrode's surface confirms the active participation of PS in the formation of

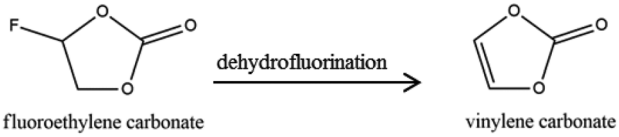

Scheme 1. Dehydrofluorination reaction of FEC generating VC and HF, which further reacts with Li ions leading to LiF formation.

© 2019 Karlsruhe Institute of Technology. Published by WILEY-VCH Verlag GmbH & Co. KGaA, Weinheim

the CEI layer. According to the literature, the peak at binding energy of 167.5 eV correspond to the detection of Li_2SO_3, while the peak at 169.6 is related to sulfite species such as RSO_3 and $ROSO_2Li$.[74] These results are in agreement with previously reported studies on the CEI layer formation on lithium-rich NMC cathode.[50] It is worth noting that the presence of sulfite species formed upon decomposition of ionic liquid-based electrolytes has been reported to have beneficial effects on the electrode cycling performance.[75]

The electrochemical performance of NMC532 electrode cycled in PS confirms the superior properties of PS with respect to the other additives. Indeed, PS acts as a scavenger of water and acidic impurities[50] in the electrolyte and consequently stabilizes $LiPF_6$ salt and carbonate electrolyte decomposition and avoids dissolution of transition metals of cathode electrode (e.g., Mn and Co) thus improving the cycling stability and CE of the positive electrode in NMC532//Li cell configuration.

2.4. Post-Mortem Scanning Electron Microscopy (SEM) Analysis of the Positive Electrodes in NMC532//Li Cells

To get insights into the morphological properties of the electrode's surface after cycling in different electrolytes, post-mortem SEM analysis has been performed on the pristine and cycled NMC532 electrodes, which results are reported in **Figure 6**.

At lower magnification, the pristine electrode exhibits the expected morphology with a homogenous distribution of active material and carbon additive, while at higher magnification the typical morphology of the layered NMC particles is also visible. Cycling the electrode in Std, an inhomogenous layer of decomposition products is observed on the electrode surface, which also shows cracks. The high magnification micrograph clearly reveals that the particles of the NMC532 electrode cycled in Std are covered and connected by a brighter layer (less electronically conductive) of compounds compared to the dark NMC532 particles. Similar features are also observed on the electrodes cycled in VC and FEC. However, the amount of species deposited on the electrodes' surface changes depending on the electrolyte following the trend FEC < VC << Std. The same trend is observed in the low magnification images, where the surface layer observed on the electrode cycled in FEC is slightly more homogenous than for those cycled in VC and Std. Interestingly, the electrode cycled in PS exhibits a very different morphology. In the low magnification micrograph, a uniform CEI layer is seen to cover most of the particles. Also, the electrode morphology (especially the distance between the NMC secondary particles) appears to be less affected by the cycling procedure with respect to the electrodes cycled in the other electrolytes. The same trend is observed in the high magnification micrograph, showing the morphology of the electrode cycled in PS to be rather similar to that of the pristine electrode. This observation correlates very well with the improved capacity retention obtained with the PS employing cells. As a matter of the fact, the high magnification image of the electrode cycled in VC, which owns the second best electrochemical performance, shows that only moderate cracking occurred, well correlating the developed electrode morphology with capacity retention and CE.

2.5. Electrochemical and Post-Mortem Analysis of NMC532//Gr Cells

The electrochemical performance of NMC532 electrodes with the four electrolytes has been investigated also in full-cell configuration employing graphite electrodes.

After the formation cycle, all cells were galvanostatically cycled at 1 C for over 120 cycles.

The galvanostatic cycling results are reported in **Figure 7** in terms of specific capacity and CE (Figure 7a) as well as the voltage profile at the 120th cycle (Figure 7b). Among all cells, those employing PS and VC show higher specific capacity over long-term cycling while the poorest performance is shown by that employing Std. After 120 cycles, the cells show CE slightly higher than 99.8% with a capacity retention over 88% for the PS and VC electrolytes, but only 84% for Std. The detailed values of capacity retention, CE, and specific capacity upon cycling of the NMC532//Gr cells are summarized in **Table 2**. Indeed, these values are substantially better than those recorded for the lithium metal cells, confirming the negative role played by the metal electrode regarding the electrolyte decomposition and CEI formation. The improved long-term stability employing graphite anode instead of metallic lithium is clearly observable by comparing Figure 7 with Figure S2 in the Supporting Information exhibiting 120 cycles of the NMC//Li half-cells.

Overall the NMC532//Gr cells exhibit slightly improved CE values at the 33rd cycle when compared to the NMC532//Li cells (see also Table 1), however, the capacity retention after 33 cycles is inferior due to the limited lithium inventory available as well as other cell balancing effects. Nonetheless, after 120 cycles the NMC532//Gr cells containing VC, FEC, and PS present all very promising values of CE and capacity retention when compared to those with Std as the electrolyte. Such an improvement is very well seen in Figure 7b comparing the voltage profile of the NMC532//Gr cells at the 120th cycle. After this cycle, the cells were disconnected in the discharged state and the lithiated NMC532 and de-lithiated graphite electrodes were recovered for post-mortem XPS analysis.

The X-ray photoelectron spectra of the recovered NMC532 electrodes are reported in **Figure 8**. C 1s region is available in Figure S1 in the Supporting Information.

The use of graphite negative electrodes clearly mitigates the electrolyte decomposition occurring on the positive electrode, independently on the electrolyte employed.

In fact, more pronounced peaks are observed in the Mn 2p region when compared to those obtained from the positive electrodes recovered from NMC532//Li cells (compare Figures 5 and 8). Furthermore, the CEI thickness trend appears to be different. Here, PS leads to the thickest CEI layer while VC, FEC, and Std exhibit thinner layers.

In the O 1s region, a new peak at ≈531 eV is detected for all samples, but not observed in NMC532//Li cells, which can be attributed to the formation of P-O bond-containing compounds such as lithium fluorophosphates.[76] Indeed, this observation is in agreement with the more pronounced high binding energy component in the F 1s region, which is attributed to Li_xPF_y and $Li_xPO_yF_z$ species. In addition, the electrode cycled in VC exhibits an extra peak in O 1s region at high binding energies attributed to the presence of oligo-VC species, not

© 2019 Karlsruhe Institute of Technology. Published by WILEY-VCH Verlag GmbH & Co. KGaA, Weinheim

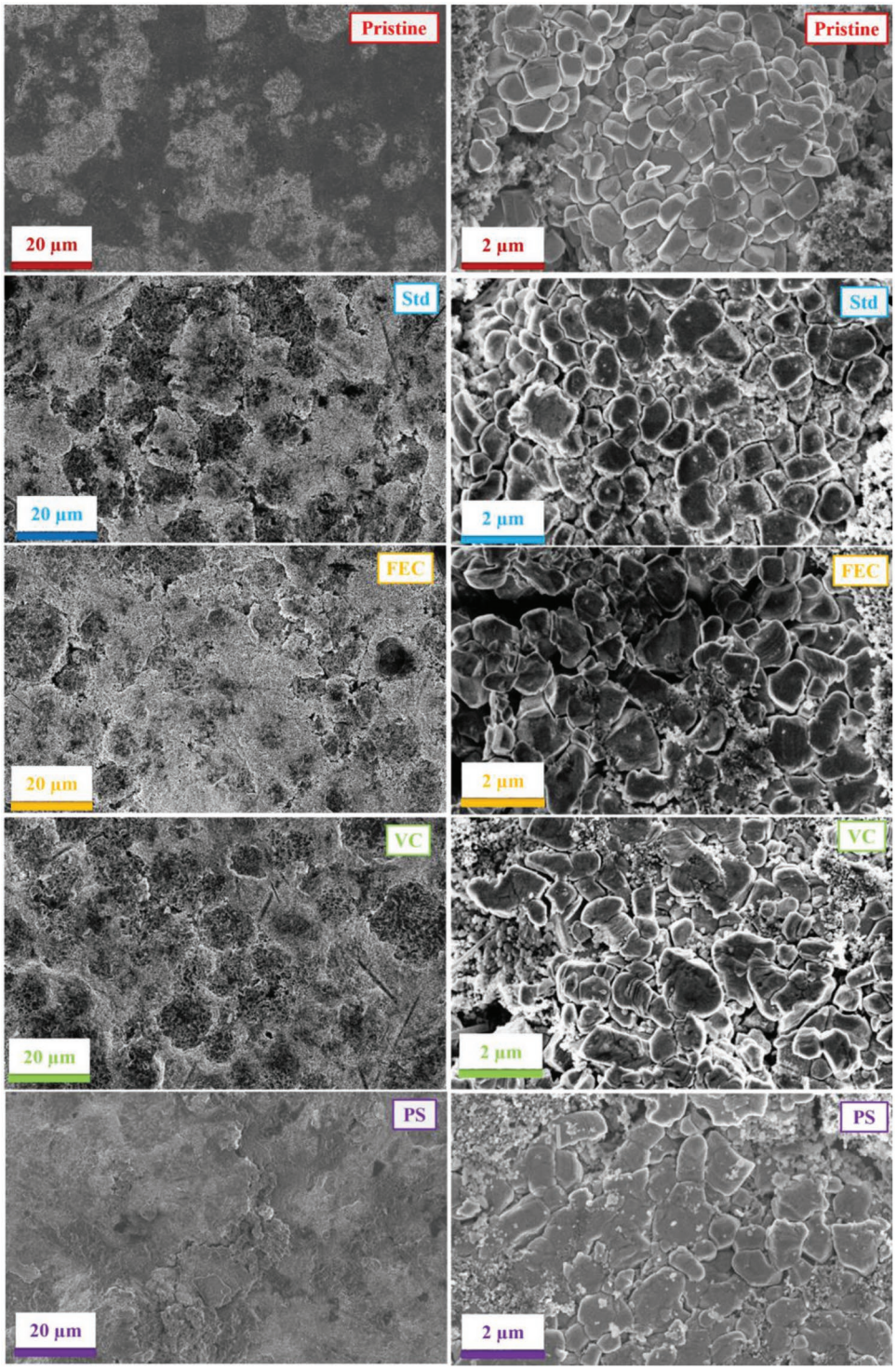

Figure 6. SEM micrographs at different magnifications of NMC532 electrodes pristine (uncycled) and recovered in the lithiated state after cycling (33rd cycle) from NMC532//Li cells employing Std, PS, VC, and FEC.

observed for the electrode cycled in FEC. The absence of this contribute, when compared to the NMC532 cycled in half-cell, is to be related with the overall lower decomposition of the electrolyte in the presence of graphite, leading to a lower presence of oligo-VC species in both VC- and FEC-containing cells.

The F 1s core level spectra show, once more, the two peaks associated with LiF (lower binding energies) and lithium fluorophosphates and C-F bonds (higher binding energies). Interestingly, the lower intensity of the LiF peak in the electrodes of the NMC532//Gr cells with respect to those from the

© 2019 Karlsruhe Institute of Technology. Published by WILEY-VCH Verlag GmbH & Co. KGaA, Weinheim

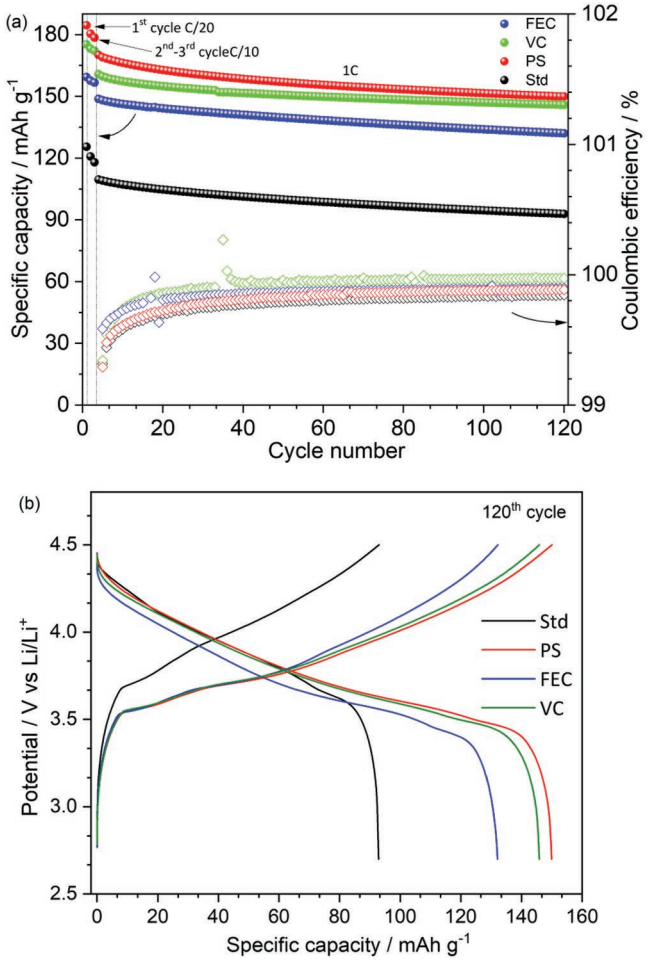

Figure 7. Cycling performance of NMC532//Gr cells employing Std, PS, VC, and FEC in terms of a) specific capacity and CE over 120 cycles and b) selected potential profiles. Test run at room temperature. Potential range: 2.7–4.5 V versus Li/Li^+.

NCM532//Li cells, indicates a lower contribution of this compound to the CEI layer, in the former cells. The effect is more pronounced in the presence of FEC, indicating a reduced salt decomposition and thus, a thinner layer generation. Indeed, despite LiF can be formed through dehydrofluorination of FEC, still the major source of LiF is the decomposition of the electrolyte salt. Due to the overall lower decomposition of FEC in NMC532//Gr cells, the LiF content is similar in all electrolytes.

The XPS S 2p peaks occurring only in the presence of PS as additive indicate the presence of RSO_3 components, confirming the active participation of PS in the CEI layer formation also in the NMC532//Gr cells.

It is worth noting that RSO_3 compounds are generally produced as reduction products[74] of PS, thus, we could expect to observe these compounds at the anode side upon de-lithiation of the full-cell. Their presence on the surface of the lithiated cathode suggests cross-talking of the electrodes within the cell, which results in the migration of decomposition components from the negative to the positive electrode and contribution to CEI layer formation. The results confirm previous studies on the cross-over effects observed in Li-ion cells.[77] Fang et al.[78] recently reported that the cross-over effects observed in NMC532//Gr cells can be significantly reduced by using lithium titanate (LTO) as anode. The anode to cathode SEI migration was significantly reduced when switching from graphite to LTO as a consequence of the decreased anode-electrolyte reactivity.

Figure 9 reports the X-ray photoelectron spectra of the graphite electrodes recovered from the NMC532//Gr cells after 120 cycles. In the C 1s region, the peak detected at lower binding energy ≈283 eV is generally attributed to partially lithiated graphite and/or underlying non lithiated graphite. The intensity of this peak can thus be considered as a good indicator for the qualitative calculation of the thickness of the SEI. According to the peak intensity, the SEI thickness decreases with the following order: VC > FEC > PS > Std. Considering that the VC and PS additives show the best cell performance in NMC532//Gr cells, the reduced SEI thickness is clearly not the optimal solution in this case. Indeed, the nature and composition of the SEI must play a key role in determining the efficiency of the electrode (de-)lithiation and charge transfer processes. The Li^+ charge transfer process generally involved in the intercalation of Li^+ ions in the host electrode includes a de-solvation step of the solvated Li^+ ions in the liquid electrolyte and a Li^+ ions transport step in the electrode/electrolyte interphase until the Li^+ ions accept electrons and become Li in the electrode.[79]

Whether the de-solvation process or the Li^+ transport through the interphases is a limiting step depends on the nature of the interphases. When the CEI/SEI is very conductive, the Li^+ charge transfer kinetics is dominated by the de-solvation process, while when the chemical nature of the interphase hinders the Li^+ ions conduction the limiting step is the Li^+ ions transport.

When an additive is introduced in the electrolyte, the Li^+ ions charge transfer process kinetics are strongly modified by the nature and amount of additive used.[80]

With the VC additive, peaks attributed to oligo-VC were again detected in both O 1s and C 1s regions, while the PS additive contributes also at the graphite side with the formation of RSO_3 and Li_2SO_3 components. It has been reported that despite being an SEI-forming additive, PS does not decompose

Table 2. Cycling parameters of NMC532//Gr full-cells cycled with Std, PS, VC, and FEC as electrolytes.

	CE at the 33rd cycle/%	Capacity retention (33rd vs 4th cycle)/%	Specific capacity at the 33rd cycle/mAh g^{-1}	CE at the 120th cycle/%	Capacity retention (120th vs 4th cycle)/%	Specific capacity at the 120th cycle/mAh g^{-1}
Std	99.75	93.4	102.4	99.84	84.7	92.9
FEC	99.84	95.5	142.1	99.89	88.8	132.1
VC	99.90	95.1	152.9	99.97	90.7	145.8
PS	99.79	93.9	159.8	99.88	88.13	149.9

© 2019 Karlsruhe Institute of Technology. Published by WILEY-VCH Verlag GmbH & Co. KGaA, Weinheim

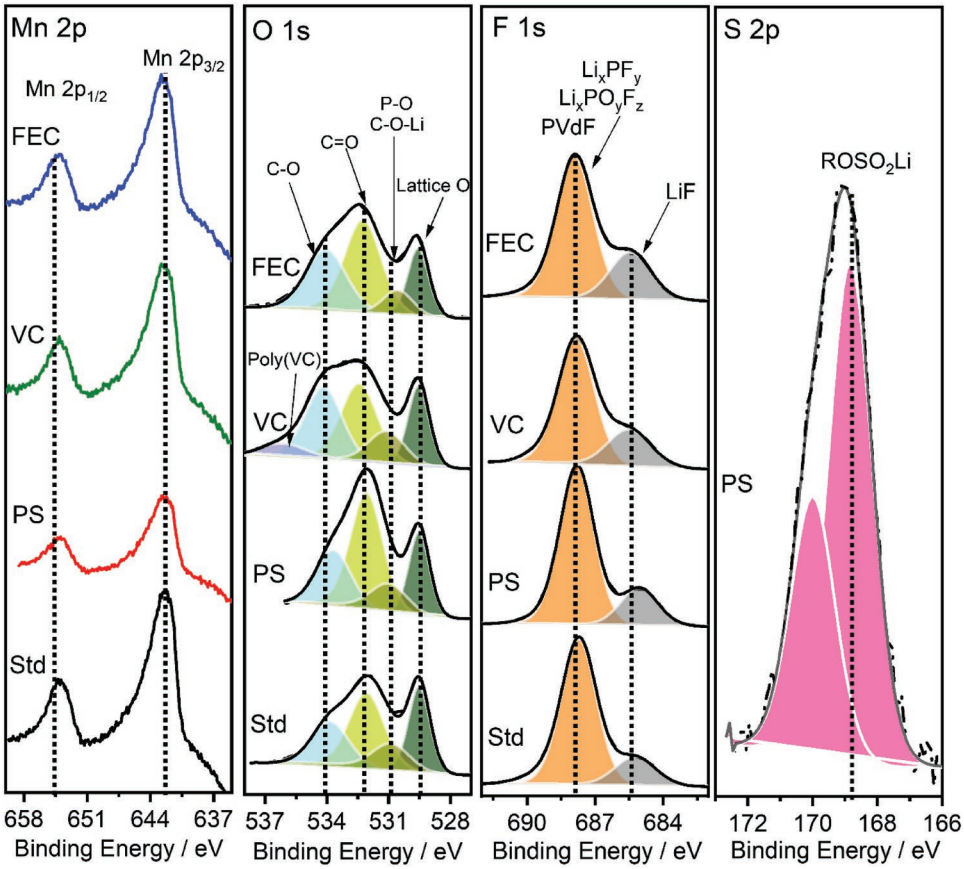

Figure 8. X-ray photoelectron core level spectra of the Mn 2p, O 1s, F 1s, and S 2p region of NMC532 electrodes recovered in the de-lithiated state after cycling (120th cycle) from NMC532//Gr cells employing Std, PS, VC, and FEC.

earlier than the other electrolyte components to form the SEI on graphite,[81] but it strongly reduces the LiF content by its HF and water impurities scavenging effect. LiF is a desirable SEI component but an excessive amount might hinder the efficient (de-)lithiation process because of its very poor ionic conductivity. By adding FEC to the electrolyte, a LiF-rich SEI layer forms on graphite explaining the poor electrochemical performance of the NMC532//Gr cells employing FEC added electrolyte.

3. Conclusion

The effect of three electrolyte additives (VC, PS, FEC) on the electrochemical performance and the CEI nature of NMC532 in cells employing Li (half-cell) and graphite (full-cell) negative electrodes was thoroughly investigated. The addition of VC and PS to the standard electrolyte (1 M $LiPF_6$ in EC:3DMC:PC solution) improves the performance of the NMC532 electrodes in both configurations in terms of delivered capacity, cycling stability, and CE. The improvement is attributed to the formation of stable and passivating CEI layers. In this work, the investigation of the NMC532//Li cells enabled a comprehensive chemical and morphological characterization of the CEI layer formed on NMC532. However, the use of metallic lithium strongly exacerbates all the processes due to its extreme reactivity toward the electrolytes, suggesting that the results are not representative for Li-ion cells, but only for Li-metal cells.

In NMC532/Gr cells, all electrolyte additives exhibit improved electrochemical performance attributable to the effective SEI and CEI layers formed on both electrodes.

The CEI layer formed on NMC532 upon cycling is thinner in graphite- than Li-cells, attesting the more stable CEI formation in the presence of the former negative electrode. The VC- and PS-containing cells show well-improved performance combined with the specific decomposition products (sulfite compounds and oligo-VC, respectively) present on both NMC532 and graphite electrodes.

The lowest improvement observed with FEC is related to lithium ions trapping resulting from the reactions with HF generated by the decomposition of FEC.

It is found that despite thickness plays a key role for the processes occurring at the CEI, the nature and chemical composition are much more important properties. Indeed, despite the surface layer formed by using VC-containing electrolyte is the thickest one among the studied electrolytes, an improved electrochemical performance is observed most likely associated with the presence of VC polymers (oligo-VC).

Moreover, the investigation of the SEI formed on the graphite electrode and the comparison with the chemical nature of the CEI layer formed on the cathode clearly reveals the occurrence of cross-talking between the two electrodes. Indeed, the detection of typical SEI reduction products on the positive electrode

 © 2019 Karlsruhe Institute of Technology. Published by WILEY-VCH Verlag GmbH & Co. KGaA, Weinheim

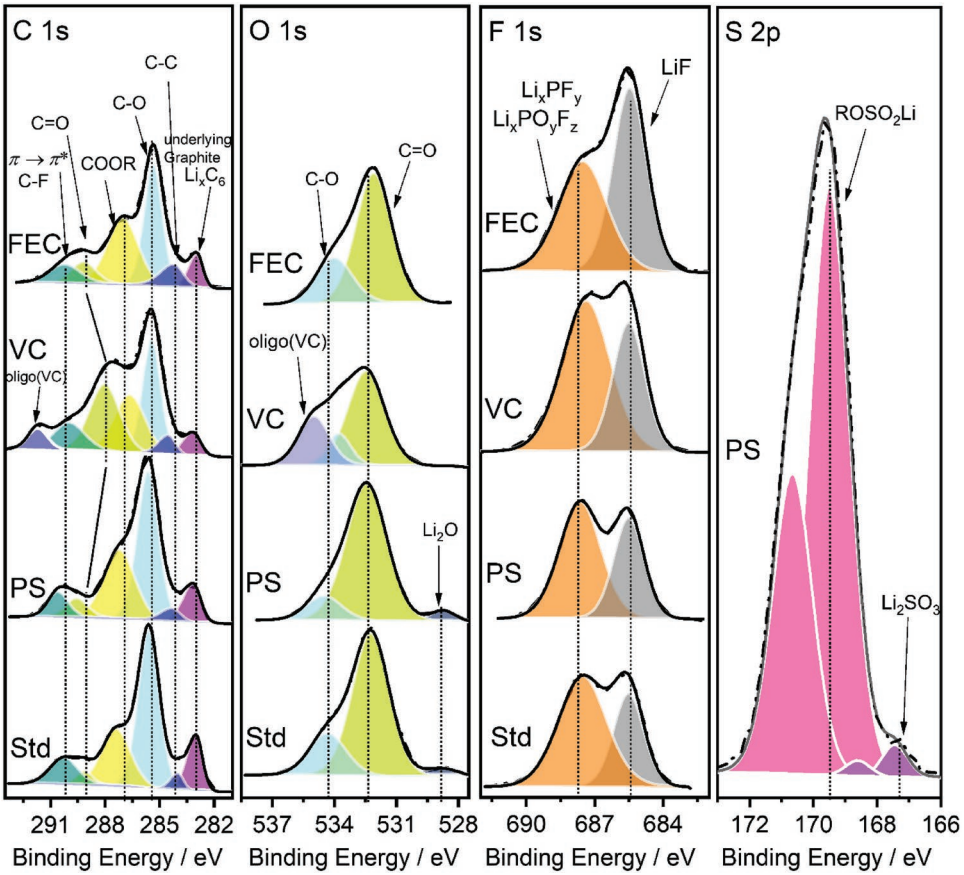

Figure 9. X-ray photoelectron core level spectra of the C 1s, O 1s, F 1s, and S 2p region of graphite electrodes recovered in the de-lithiated state after cycling (120th cycle) from NMC532//Gr cells employing Std, PS, VC, and FEC.

surface confirms the migration of decomposition components from the negative to the positive electrode and contribution to CEI layer formation. The processes occur both with lithium and graphite anodes, however in the latter case the amount of decomposition products is mitigated attesting for the increased reactivity of lithium metal with respect to graphite.

4. Experimental Section

Electrode Preparation: NMC532 electrodes were prepared by doctor-blade casting the slurry, which dry composition was 88 wt% active material, 7 wt% conductive carbon (Super C65, Imerys, Switzerland), and 5 wt% binder (PVdF, 6020 Solef, Solvay) onto a 20 µm thick aluminium foil (UACJ). First, PVdF was dissolved beforehand in *N*-methyl-2-pyrrolidone (Sigma-Aldrich) for 12 h in a 1:9 weight ratio. Then the active material and conductive carbon were added. The resulting slurry was stirred for 12 h at 300 rpm to ensure homogenous mixing. After coating, the electrode tapes were dried overnight at 80 °C. Then, 12 mm diameter electrodes were punched and dried at 120 °C under vacuum for 12 h before being transferred to argon-filled glove box (O_2 and H_2O levels below 0.1 ppm, MBraun, Stratham, NH, USA) for cell assembly. The average active material mass loading was ≈5 mg cm^{-2}.

The graphite electrode slurry consisted of 95 wt% graphite (SLP30, Imerys, Switzerland), 1 wt% conductive carbon C-NERGY Super C45 (Imerys, Switzerland) and 2 wt% Na-CMC (CRT 30000 PA 09, Walocel, Dow Wolff Cellulosics, Germany), and 2% styrene butadiene rubber (SBR, TRD 102A, JSR Micro, USA) as binders. The slurry was prepared by first dissolving Na-CMC in pure water by stirring for 1.5 h. Then Super C45 and graphite were consecutively added mixing for 2 h after each addition. The mixture was then stirred and sonicated for three intervals of 1 min in an ultrasonic bath. In the last step, SBR (aqueous dispersion) was added to the mixture and mixed for 1 h. The resulting slurry was doctor-blade cast onto copper foil (20 µm) and dried in an 80 °C oven overnight. Afterward, 12 mm diameter electrodes were punched, dried, and stored in a glove box (similarly to NMC532 electrodes). The average active material mass loading was ≈2 mg cm^{-2}.

Cell Assembly and Electrochemical Tests: The electrochemical tests of the NMC//Li cells were performed by assembling coin cells (type 2032) in an argon-filled glove box. The lithium half-cells were assembled using NMC532 electrodes as working electrode and 14 mm ∅ metallic lithium foil disks (Rockwood, ALBEMARLE, Charlotte, NC, USA) as counter electrode (CE). Glass fiber disks (GF/D, ∅ = 16 mm) were used as separator wetted with 100 µL electrolyte solution and added to each cell. 1 M $LiPF_6$ dissolved in EC (ethylene carbonate, BASF):DMC (dimethyl carbonate, UBE):PC (propylene carbonate, BASF) in a 1:3:1 volume ratio was used as standard electrolyte. For the additive-containing electrolytes, 2 wt% of VC (Solvionic, 99%), PS (Alfa Aesar, 99%), or FEC (BASF) were added into the standard electrolyte. Within the manuscript, the standard and additive-containing electrolytes were shortly named as Std, VC, FEC, and PS. The electrolyte solutions were prepared inside an argon-filled glove box, mixed overnight, and transferred and stored into aluminium bottles.

NMC532//Gr full-cells were assembled using three-electrode T-type Swagelok cells with 120 µL electrolyte impregnated in glass fiber disks (GF/D, ∅ = 14 mm) used as separator. Graphite, NMC532, and lithium were used as counter, working, and reference electrodes, respectively. The graphite to NMC532 capacity ratio was adjusted to ≈1.2.

All electrochemical characterizations were performed at room temperature (20 ± 1 °C) using a climatic chamber (Binder GmbH, KB 400).

© 2019 Karlsruhe Institute of Technology. Published by WILEY-VCH Verlag GmbH & Co. KGaA, Weinheim

Constant current cycling tests were performed using a battery cycler (Series 4000, Maccor, USA). The cycling test consisted of a series of charge/discharge cycles at 1 C rate (1 C rate for the cathode corresponds to a current of 160 mA g^{-1}) within the 4.5–3.0 V (vs Li/Li^+ only in the three-electrode cells) range after an initial formation protocol including a first cycle at C/20 rate followed by two cycles at C/10 rate.

The anodic stability of the electrolytes was investigated using working electrodes containing carbon black. These were prepared as the graphite electrodes but employing only the conductive carbon and PVdF in the 75:25 weight ratio. Three electrode cells were realized as described above. Linear sweep voltammetries from OCP up to 6 V (vs Li/Li^+) were performed using a multichannel galvanostat-potentiostat (VMP, BioLogic) with a scan rate of 0.1 mV s^{-1}.

Electrode Characterization: Post-mortem analysis was performed on cycled electrodes, which were recovered from fully discharged (3 V) cells. The lithiated NMC532 and de-lithiated graphite electrodes were extracted from the cells inside an argon glove box, rinsed with 200 µL of DMC (BASF) to remove residual electrolyte, and dried under vacuum for 30 min at room temperature.

XPS characterization was carried out in SPECS UHV system (FOCUS 500 monochromated X-ray source, PHOIBOS 150 hemispherical energy analyzer with 1D DLD detector) using the Al-Kα (1486.6 eV) radiation. The measurements were performed using pass energies at the analyzer of 60 and 30 eV for survey and detail spectra, respectively. The X-ray photoelectron spectra for NMC532 and graphite were calibrated to the signal of amorphous carbon (Super C65) at 284.8 eV and graphitic carbon at 284.4, respectively, and de-convoluted and analyzed employing CasaXPS software.

The morphology of the recovered electrodes was probed using a Zeiss LEO 1550 VP field emission SEM (FE-SEM Carl Zeiss, Germany).

Supporting Information

Supporting Information is available from the Wiley Online Library or from the author.

Acknowledgements

The authors acknowledge Imerys and Rockwood Lithium for providing C-NERGY conductive carbon and lithium foil, respectively. The financial support from the EU under the grant agreement no. 653373 (SPICY—Silicon and polyanionic chemistries and architectures of Li-ion cell for high energy battery, H2020-GV-2014). R.E. acknowledges DAAD and BMBF for the support within the KHYS. The support of the Helmholtz Association is also acknowledged.

Conflict of Interest

The authors declare no conflict of interest.

Keywords

cathode/electrolyte interface, electrolyte additive, lithium-ion battery, NMC, X-ray photoelectron spectroscopy

Received: August 31, 2019
Revised: October 21, 2019
Published online:

[1] C. Iclodean, B. Varga, N. Burnete, D. Cimerdean, B. Jurchiş, *IOP Conf. Ser.: Mater. Sci. Eng.* **2017**, *252*, 012058.
[2] S. J. Gerssen-Gondelach, A. P. C. Faaij, *J. Power Sources* **2012**, *212*, 111.
[3] A. Sakti, J. J. Michalek, E. R. H. Fuchs, J. F. Whitacre, *J. Power Sources* **2015**, *273*, 966.
[4] Y. Nishi, *Chem. Rec.* **2001**, *1*, 406.
[5] A. Yoshino, *Angew. Chem., Int. Ed.* **2012**, *51*, 5798.
[6] T. B. Reddy, D. Linden, *Linden's Handbook of Batteries*, McGraw Hill, New York **2011**.
[7] M. Armand, J.-M. Tarascon, *Nature* **2008**, *451*, 652.
[8] S. S. Zhang, *J. Power Sources* **2006**, *162*, 1379.
[9] J. B. Goodenough, *J. Power Sources* **2007**, *174*, 996.
[10] I. Belharouak, Y. K. Sun, J. Liu, K. Amine, *J. Power Sources* **2003**, *123*, 247.
[11] M. S. Whittingham, *Chem. Rev.* **2004**, *104*, 4271.
[12] J. Choi, A. Manthiram, *J. Electrochem. Soc.* **2005**, *152*, A1714.
[13] H. Gabrisch, T. Yi, R. Yazami, *Electrochem. Solid-State Lett.* **2008**, *11*, A119.
[14] W. Liu, P. Oh, X. Liu, M. J. Lee, W. Cho, S. Chae, Y. Kim, J. Cho, *Angew. Chem., Int. Ed.* **2015**, *54*, 4440.
[15] H.-J. Noh, S. Youn, C. S. Yoon, Y.-K. Sun, *J. Power Sources* **2013**, *233*, 121.
[16] D. Andre, S. J. Kim, P. Lamp, S. F. Lux, F. Maglia, O. Paschos, B. Stiaszny, *J. Mater. Chem. A* **2015**, *3*, 6709.
[17] N. Nitta, F. Wu, J. T. Lee, G. Yushin, *Mater. Today* **2015**, *18*, 252.
[18] D. Larcher, J.-M. Tarascon, *Nat. Chem.* **2015**, *7*, 19.
[19] R. Jung, M. Metzger, F. Maglia, C. Stinner, H. A. Gasteiger, *J. Electrochem. Soc.* **2017**, *164*, A1361.
[20] S. K. Jung, H. Gwon, J. Hong, K. Y. Park, D. H. Seo, H. Kim, J. Hyun, W. Yang, K. Kang, *Adv. Energy Mater.* **2014**, *4*, 1.
[21] K.-S. Lee, S.-T. Myung, K. Amine, H. Yashiro, Y.-K. Sun, *J. Electrochem. Soc.* **2007**, *154*, A971.
[22] Y.-K. Sun, H.-J. Noh, C. S. Yoon, *J. Electrochem. Soc.* **2011**, *159*, A1.
[23] B. J. Hwang, Y. W. Tsai, C. H. Chen, R. Santhanam, *J. Mater. Chem.* **2003**, *13*, 1962.
[24] Y.-K. Sun, H.-B. Kang, S.-T. Myung, J. Prakash, *J. Electrochem. Soc.* **2010**, *157*, A1335.
[25] H.-G. Kim, S.-T. Myung, J. K. Lee, Y.-K. Sun, *J. Power Sources* **2011**, *196*, 6710.
[26] P. Hou, J. Yin, M. Ding, J. Huang, X. Xu, *Small* **2017**, *13*, 1701802.
[27] D. R. Gallus, R. Schmitz, R. Wagner, B. Hoffmann, S. Nowak, I. Cekic-Laskovic, R. W. Schmitz, M. Winter, *Electrochim. Acta* **2014**, *134*, 393.
[28] H. Zheng, Q. Sun, G. Liu, X. Song, V. S. Battaglia, *J. Power Sources* **2012**, *207*, 134.
[29] J. Wandt, A. Freiberg, R. Thomas, Y. Gorlin, A. Siebel, R. Jung, H. A. Gasteiger, M. Tromp, *J. Mater. Chem. A* **2016**, *4*, 18300.
[30] Z. Chen, D. Chao, J. Lin, Z. Shen, *Mater. Res. Bull.* **2017**, *96*, 491.
[31] Z. Chen, G. T. Kim, D. Bresser, T. Diemant, J. Asenbauer, S. Jeong, M. Copley, R. J. Behm, J. Lin, Z. Shen, S. Passerini, *Adv. Energy Mater.* **2018**, *8*, 1.
[32] E. Peled, *J. Electrochem. Soc.* **1979**, *126*, 2047.
[33] D. Y. Wang, J. Xia, L. Ma, K. J. Nelson, J. E. Harlow, D. Xiong, L. E. Downie, R. Petibon, J. C. Burns, A. Xiao, W. M. Lamanna, J. R. Dahn, *J. Electrochem. Soc.* **2014**, *161*, A1818.
[34] B. Zhang, M. Metzger, S. Solchenbach, M. Payne, S. Meini, H. A. Gasteiger, A. Garsuch, B. L. Lucht, *J. Phys. Chem. C* **2015**, *119*, 11337.
[35] D. Aurbach, K. Gamolsky, B. Markovsky, Y. Gofer, M. Schmidt, U. Heider, *Electrochim. Acta* **2002**, *47*, 1423.
[36] H. Ota, K. Shima, M. Ue, J. Yamaki, *Electrochim. Acta* **2004**, *49*, 565.
[37] M. Contestabile, M. Morselli, R. Paraventi, R. Neat, *J. Power Sources* **2003**, *119–121*, 943.
[38] M. Holzapfel, C. Jost, A. Prodi-Schwab, F. Krumeich, A. Würsig, H. Buqa, P. Novák, *Carbon* **2005**, *43*, 1488.
[39] E. G. Shim, T. H. Nam, J. G. Kim, H. S. Kim, S. I. Moon, *J. Power Sources* **2007**, *172*, 901.

 © 2019 Karlsruhe Institute of Technology. Published by WILEY-VCH Verlag GmbH & Co. KGaA, Weinheim

[40] L. Chen, K. Wang, X. Xie, J. Xie, *J. Power Sources* **2007**, *174*, 538.
[41] M. Nie, J. Demeaux, B. T. Young, D. R. Heskett, Y. Chen, A. Bose, J. C. Woicik, B. L. Lucht, *J. Electrochem. Soc.* **2015**, *162*, A7008.
[42] J. C. Burns, R. Petibon, K. J. Nelson, N. N. Sinha, A. Kassam, B. M. Way, J. R. Dahn, *J. Electrochem. Soc.* **2013**, *160*, A1668.
[43] J. C. Burns, G. Jain, A. J. Smith, K. W. Eberman, E. Scott, J. P. Gardner, J. R. Dahn, *J. Electrochem. Soc.* **2011**, *158*, A255.
[44] L. Madec, R. Petibon, J. Xia, J.-P. Sun, I. G. Hill, J. R. Dahn, *J. Electrochem. Soc.* **2015**, *162*, A2635.
[45] L. Madec, J. Xia, R. Petibon, K. J. Nelson, J.-P. Sun, I. G. Hill, J. R. Dahn, *J. Phys. Chem. C* **2014**, *118*, 29608.
[46] L. El Ouatani, R. Dedryvère, C. Siret, P. Biensan, S. Reynaud, P. Iratçabal, D. Gonbeau, *J. Electrochem. Soc.* **2009**, *156*, A103.
[47] L. El Ouatani, R. Dedryvère, C. Siret, P. Biensan, D. Gonbeau, *J. Electrochem. Soc.* **2009**, *156*, A468.
[48] J. Xia, J. E. Harlow, R. Petibon, J. C. Burns, L. P. Chen, J. R. Dahn, *J. Electrochem. Soc.* **2014**, *161*, A547.
[49] X. Zuo, M. Xu, W. Li, D. Su, J. Liu, *Electrochem. Solid-State Lett.* **2006**, *9*, A196.
[50] A. Birrozzi, N. Laszczynski, M. Hekmatfar, J. Von Zamory, G. A. Giffin, S. Passerini, *J. Power Sources* **2016**, *325*, 525.
[51] J. Pires, L. Timperman, A. Castets, J. S. Peña, E. Dumont, S. Levasseur, R. Dedryvère, C. Tessier, M. Anouti, *RSC Adv.* **2015**, *5*, 42088.
[52] R. McMillan, H. Slegr, Z. X. Shu, W. Wang, *J. Power Sources* **1999**, *81–82*, 20.
[53] H. Nakai, T. Kubota, A. Kita, A. Kawashima, *J. Electrochem. Soc.* **2011**, *158*, A798.
[54] A. Bordes, K. Eom, T. F. Fuller, *J. Power Sources* **2014**, *257*, 163.
[55] H. Shin, J. Park, A. M. Sastry, W. Lu, *J. Electrochem. Soc.* **2015**, *162*, A1683.
[56] D. Y. Wang, N. N. Sinha, J. C. Burns, C. P. Aiken, R. Petibon, J. R. Dahn, *J. Electrochem. Soc.* **2014**, *161*, A467.
[57] C. Xu, G. Hernández, S. Abbrent, L. Kobera, R. Konefal, J. Brus, K. Edström, D. Brandell, J. Mindemark, *ACS Appl. Energy Mater.* **2019**, *2*, 4925.
[58] Y. Qian, P. Niehoff, M. Börner, M. Grützke, X. Mönnighoff, P. Behrends, S. Nowak, M. Winter, F. M. Schappacher, *J. Power Sources* **2016**, *329*, 31.
[59] J. Li, H. Li, W. Stone, S. Glazier, J. R. Dahn, *J. Electrochem. Soc.* **2018**, *165*, A626.
[60] D. Moosbauer, S. Zugmann, M. Amereller, H. J. Gores, *J. Chem. Eng. Data* **2010**, *55*, 1794.
[61] J. Kasnatscheew, M. Evertz, B. Streipert, R. Wagner, R. Klöpsch, B. Vortmann, H. Hahn, S. Nowak, M. Amereller, A. C. Gentschev, P. Lamp, M. Winter, *Phys. Chem. Chem. Phys.* **2016**, *18*, 3956.
[62] O. Dolotko, A. Senyshyn, M. J. Mühlbauer, K. Nikolowski, H. Ehrenberg, *J. Power Sources* **2014**, *255*, 197.
[63] K. M. Shaju, G. V. Subba Rao, B. V. R. Chowdari, *Electrochim. Acta* **2002**, *48*, 145.
[64] P. van der Heide, *X-Ray Photoelectron Spectroscopy: An Introduction to Principles and Practices*, John Wiley & Sons, New York **2011**.
[65] S. Tanuma, C. J. Powell, D. R. Penn, *Surf. Interface Anal.* **1991**, *17*, 927.
[66] S. Tanuma, C. J. Powell, D. R. Penn, *Surf. Interface Anal.* **1994**, *21*, 165.
[67] S. E. Renfrew, B. D. McCloskey, *J. Am. Chem. Soc.* **2017**, *139*, 17853.
[68] R. Dedryvère, L. Gireaud, S. Grugeon, S. Laruelle, J. M. Tarascon, D. Gonbeau, *J. Phys. Chem. B* **2005**, *109*, 15868.
[69] S. Malmgren, K. Ciosek, M. Hahlin, T. Gustafsson, M. Gorgoi, H. Rensmo, K. Edström, *Electrochim. Acta* **2013**, *97*, 23.
[70] L. Madec, R. Petibon, K. Tasaki, J. Xia, J.-P. Sun, I. G. Hill, J. R. Dahn, *Phys. Chem. Chem. Phys.* **2015**, *17*, 27062.
[71] L. Baggetto, D. Mohanty, R. A. Meisner, C. A. Bridges, C. Daniel, D. L. Wood III, N. J. Dudney, G. M. Veith, *RSC Adv.* **2014**, *4*, 23364.
[72] P. Niehoff, S. Passerini, M. Winter, *Langmuir* **2013**, *29*, 15813.
[73] M. Herstedt, A. M. Andersson, H. Rensmo, H. Siegbahn, K. Edström, *Electrochim. Acta* **2004**, *49*, 4939.
[74] J. Self, D. S. Hall, L. Madec, J. R. Dahn, *J. Power Sources* **2015**, *298*, 369.
[75] F. Mueller, N. Loeffler, G. T. Kim, T. Diemant, R. J. Behm, S. Passerini, *ChemSusChem* **2016**, *9*, 1290.
[76] L. Ma, L. Ellis, S. L. Glazier, X. Ma, Q. Liu, J. Li, J. R. Dahn, *J. Electrochem. Soc.* **2018**, *165*, A891.
[77] K. W. Knehr, T. Hodson, C. Bommier, G. Davies, A. Kim, D. A. Steingart, *Joule* **2018**, *2*, 1146.
[78] S. Fang, D. Jackson, M. L. Dreibelbis, T. F. Kuech, R. J. Hamers, *J. Power Sources* **2018**, *373*, 184.
[79] T. R. Jow, S. A. Delp, J. L. Allen, J. P. Jones, M. C. Smart, *J. Electrochem. Soc.* **2018**, *165*, A361.
[80] Q. Q. Liu, R. Petibon, C. Y. Du, J. R. Dahn, *J. Electrochem. Soc.* **2017**, *164*, A1173.
[81] L. Lin, K. Yang, R. Tan, M. Li, S. Fu, T. Liu, H. Chen, F. Pan, *J. Mater. Chem. A* **2017**, *5*, 19364.

 © 2019 Karlsruhe Institute of Technology. Published by WILEY-VCH Verlag GmbH & Co. KGaA, Weinheim